Dynamic modelling for a submerged freeze microgripper using thermal networks.

Beatriz Lopez-Walle, Michaël Gauthier, Nicolas Chaillet

Dynamic modelling for a submerged freeze microgripper using thermal networks

Beatriz López-Walle‡, Michaël Gauthier and Nicolas Chaillet

FEMTO-ST Institute, UMR CNRS 6174 - UFC/ENSMM/UTBM, Automatic Control and MicroMechatronic Systems Departement (AS2M), 24 rue Alain Savary, 25000 Besançon, France

E-mail: michael.gauthier@femto-st.fr

Abstract. The growing interest for micromanipulation systems requires efficient, reliable and flexible handling strategies. Recent studies have demonstrated that performing manipulations and assembly in liquid surroundings is more advantageous than in dry conditions, especially when objects are under $100\,\mu$m in size. The thermally actuated ice microgripper proposed and analysed in this paper is designed to operate in a completely submerged manner in an aqueous medium. The handling principle which benefits from adhesive properties of ice, its thermal control principle based on Peltier effect, some features of the prototype, and the first micromanipulation tests are summarized. This paper is focused on the modelling of the thermal microhandling system using electrical analogy. The submerged microgripper is split into different subsystems which are studied in order to identify their thermal network. Then they are interconnected to build the whole thermal network of the submerged microgripper. This model is validated by comparison with experimental measurements. Controlling the temperatures involved in our device will be the purpose of further works.

‡ Current address: CIIDIT - Universidad Autónoma de Nuevo León, PIIT Monterrey, C.P. 66600, Nuevo León, Mexico.

1. Introduction

A trend grows since several years towards the automation of manipulation and assembly processes in the micro scale, i.e. typically between one micrometer and one millimeter. Their main applications are microrobotics, biological manipulations, optical, mechanical, or electrical microcomponents assembly. One of the common problems is the development of reliable and high accuracy handling strategies [1], particularly during the release phase. Without properly releasing strategies, this process can be very tedious and time-costly [2,3]. When the dimension of the object is under 100 μm, the release phase is strongly disturbed by the surrounding medium [3–6]. A comparative modelling of micromanipulation conditions in dry and liquid media, considering surface forces, contact force and hydrodynamic force, shows that manipulating in submerged conditions is more favorable than in dry conditions [7–9]. Firstly, capillary force is completely cancelled in submerged conditions. Secondly, contact force (pull-off force) and surface forces (van der Waals force, electrostatic force) reduce significantly in liquid medium. Thirdly, hydrodynamic force increases in submerged environment. These phenomena have two important consequences: they reduce drastically electrostatic and adhesion perturbations, and they limit the maximal velocity of the micro-objects and thus reduce their loss rate.

We developed a novel thermally controlled phase changing (liquid-solid) microgripper able to work in an aqueous medium. Its principle is detailed in [10] and summarized below. Current ice grippers act in air and its miniaturization is usually limited by the capillary force [11–16]. The dimensions of gripped objects are typically bigger than 200 μm and the main applications are optical, mechanical, or electrical microcomponents assembly [13]. Their thermal principle is based either on Peltier effect, or Joule-Thompson effect. As they work in air, water must be provided by an external device. Capillary force appears during the release because water does not evaporate completely. Then, they have to be combined with other release strategies to detach manipulated objects. In addition, they must work with particular environmental conditions like low temperature and low humidity [11,17].

Features of capillary grippers [18–21] and droplet based microgrippers [22, 23] are similar to cryogenic grippers. These strategies are conceived as non-destructive manipulation methods, causing no mechanical damage to the object. Many external release techniques have been tested to facilitate object release [21]. In addition, numbers of efforts are done searching for controlling the contact angle between the liquid bridge and the gripper surface, and the liquid bridge and the substrate, including regulating the liquid volume [24,25], controlling the gripper surface [18,20], and electrowetting [21,26]. None of them is general or versatile enough being necessary deep analysis and new strategies. Miniaturization is also limited because of the adhesion perturbations during the release phase.

The handling abilities of the cryogenic grippers are almost independent of the object shape. They provide high holding forces ($\approx$ 0.1 N-100 N [11, 27, 28]) but local stresses

can also be very high, damaging delicate micro-objects. It is recommended that the manipulated microcomponent can withstand low temperatures and should not be liable to rust. Inserting it into the water container, recuperating it, and drying it will be analyzed. In addition, the water temperature must be relatively close to the fusion temperature (< 283 K).

Our microgripper takes particularly advantages of the cancellation of the capillary force in submerged medium. Consequently, it can be efficiently used to manipulate objects whose size is smaller than 100 μm.

A study of the thermal exchanges in the submerged ice microgripper is necessary to predict and control its performances. In this paper we propose to develop the complete model using electrical analogy. Electrical analogy has been largely used in several areas with good results [29–34].

This paper is composed of the following sections: section 2 presents the handling and thermal principles of the submerged ice microgripper and the features of the prototype; thermal modelling via electrical analogy of the Peltier modules and the MicroPelt's heat sink is treated in section 3; ice generation is analyzed in section 4; finally, the dynamic thermal model of the whole microgripper is built and experimentally validated in section 5.

2. The submerged ice microgripper

A prototype of the submerged freeze microgripper has been developed. This section presents the handling and thermal principles, and the physical and technical features. It summarizes the detailed description proposed in [10].

2.1. Handling Principle

The handling principle of the submerged freeze microgripper uses adhesive properties of ice as shown in figure 1. First, the gripper approaches the micro-object without touching it. Secondly, an ice microvolume is generated and holds the micro-object. This latter can then be moved and positioned. Finally, the ice microvolume is thawed liberating the micro-object without any capillary force influence because ice mixes with water surroundings.

Liquid environment is thus exploited to generate the ice microvolume, and to avoid capillary force during the release.

2.2. Thermal Principle

The energy required to generate the ice microvolume of the submerged gripper is provided by two Peltier modules. When an electrical current is applied to the Peltier module, it generates heat on the hot face and absorbs heat on the cold face. The heat flux is proportional to the current. The hot face is usually associated to a heat sink in
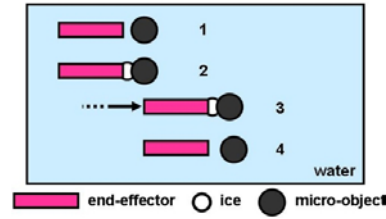
Figure 1. Handling strategy: (1) the microgripper approaches, (2) an ice microvolume is generated and catches the object, (3) the object is manipulated, (4) the ice thaws and the object is liberated.

order to dissipate the heat flux.

The submerged freeze system consists of two Peltier modules and a forced convection system as illustrated in figure 2. The first stage contains a Peltier micromodule named MicroPelt^{TM} (μP). The ice microvolume is generated on its cold face. In order to actively decrease the temperature at the MicroPelt's heat sink, a second Peltier element is connected. We called it MiniPeltier (mP). The temperature at its hot face is maintained at the ambient temperature by forced convection.

The MicroPelt is completely submerged while the MiniPeltier and the forced convection system stay in air to dissipate heat outside water.
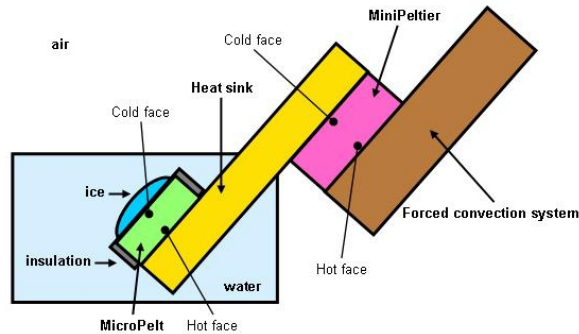

Figure 2. Submerged freeze system principle.

2.3. Physical and Technical Features

Figure 3 shows the first prototype of the submerged freeze microgripper.

The dimensions of the MicroPelt^{TM} (Infineon Technologies AG) are: $720 \times 720 \times 428$ μm^3. Its hot face is fastened to a copper heat sink (MicroPelt's heat sink). The MiniPeltier (Melcor FC0.6-18-05), which dimensions are $6.2 \times 6.2 \times 2.4$ mm^3, is fixed on its cold face to the MicroPelt's heat sink and on its hot face to the copper heat sink of the cooling liquid system.
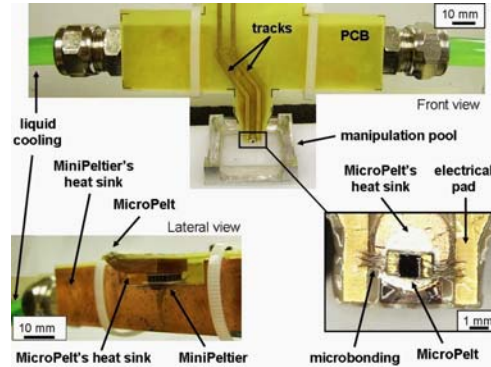
Figure 3. Experimental changing phase gripper.

Concerning power consumption, for optimal conditions operations, the MiniPeltier and the MicroPelt require 1.6 W and 0.1 W, respectively. The submerged freeze microgripper requires low power consumption compared to microgrippers using other common actuation methods (electrostatic, piezoelectric, shape memory alloy effect, etc.) [35].

Pick and place operations of a silicon micro-object ($600 \times 600 \times 100 \ \mu m^3$) are described in [10].

Under water, the maximal lifting force can be estimated with good accuracy only by knowing the contact surface between the ice droplet and the object, and the gripping strength of ice (typically around 1 N/mm^2) [11, 13, 28, 36]. Considering the MicroPelt's cold surface (0.52 mm^2) as the contact surface, this force is around 0.52 N.

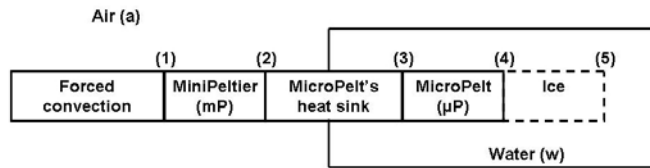## 3. Thermal modelling by electrical analogy

Predict and control the temperature distribution in the submerged freeze microgripper require a complete study of the heat exchanges. Equivalent electrical models, so-called thermal networks, seem a relatively simple, but sufficiently accurate and powerful tool for simulating real thermal systems [29, 32–34]. Furthermore, elementary thermal networks can easily be connected together. We use this faculty to split the submerged microgripper in different subsystems. The thermal networks of each subsystem considered is built and identified. They are then interconnected with the others, in order to build the complete thermal network of the microgripper. Classical equivalences between thermal and electrical systems are summarized in table 1.

The submerged freeze microgripper can be schematized as presented in figure 4, where: (a) corresponds to air; (w) corresponds to water; (1) denotes the junction between the forced convection system and the MiniPeltier's hot face; (2) represents the junction between the MiniPeltier's cold face and one side of the MicroPelt's heat sink; (3) is the junction of the MicroPelt's hot face and its heat sink; (4) is the MicroPelt's

Table 1. Thermal and electrical analogy

Thermal system	Equivalent electrical system
Heat flux Q	Current i
Temperature difference ΔT	Voltage difference ΔV

cold face; and (5) represents the surface of the ice microvolume in contact with water. These notations will be used to identify the parameters of the thermal networks.

Figure 4. Freeze microgripper's schema for identification of the parameters of the thermal networks.

According to [10], the forced convection system maintains constant the temperature of the MiniPeltier's hot face T_1 at the ambient temperature T_a. Consequently, its thermal modelling corresponds to the expression: $T_1 = T_a$.

The structure and the identification of physical parameters of both Peltier modules (MiniPeltier and MicroPelt), and the MicroPelt's heat sink's thermal networks are presented in the following.

3.1. Thermal network of Peltier modules

A Peltier module's thermal network, proposed by [12], is shown in figure 5. It consists of a current source $P_S = \alpha T_c i$ representing the Peltier effect, two current sources $P_{J/2} = Ri^2/2$ for the Joule effect, and a thermal resistance R_{TH} which represents the conduction. The Peltier coefficient α, the electrical resistance R and the thermal conductance k_P depend on the physical features of the Peltier module. i is the applied electrical current; T_h and T_c are the temperatures at the hot and cold faces, respectively; Q_h is the heat rejected by the hot face, while Q_c represents the heat absorbed by the cold face.

Classical identification methods have been used to determine the MiniPeltier's parameters. The MicroPelt's parameters have been calculated on the basis of technical parameters provided by the constructor (Infineon Technologies AG). These data are summarized in table 2.
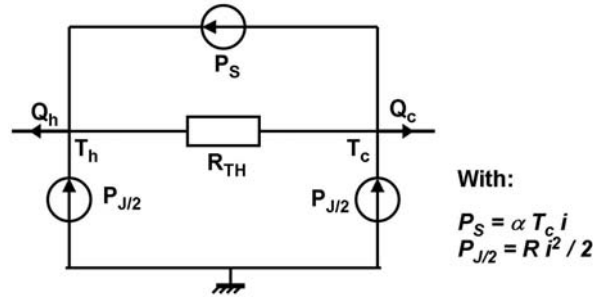
Figure 5. Thermal network for a Peltier element [12].

Table 2. Parameters of thermal networks of MiniPeltier and MicroPelt.

Parameter	MiniPeltier	MicroPelt
Peltier coefficient α (V/K)	0.007	0.001
Electrical resistance R (Ω)	1.12	0.2
Thermal resistance R_{TH} (K/W)	62.5	122

3.2. Thermal network of the MicroPelt's heat sink

The geometry and the thermal problem of the MicroPelt's heat sink is shown in figure 6. MicroPelt's hot face is fixed to surface (2), while MiniPeltier's cold face is fixed to surface (3). As the length of the heat sink is larger than all the other dimensions, we consider that the variation of the temperature between surface (2) at temperature T_2, and surface (3) at temperature T_3 is unidirectional along axis x. Consequently, the heat flux $Q(x,t)$ between both surfaces is also unidirectional. Moreover, heat convection Q_h takes place from all others surfaces and two different surroundings, air and water (see figure 4). External temperature T_{ext} involves thus both external fluids temperatures, air temperature T_a and water temperature T_w.

This thermal problem has been solved in [37]. Here, a dynamic thermal network for the MicroPelt's heat sink is proposed (see figure 7): R_{c0} is the thermal conduction resistance, R_{v0} is the thermal convection resistance, C_{th0} are the thermal capacitors, T_{ext} is the external temperature, and Q_2 and Q_3 are the heat flux in surface (2) and (3), respectively. The expressions of this parameters in the case of a rectangular beam are proposed in [37]. As the MicroPelt's heat sink is partially submerged, the external temperature T_{ext} in the thermal network is the average temperature between the temperature of the water and the temperature of the air. The identification of the thermal resistances R_{c0} and R_{v0} and the temperature T_{ext} have been obtained using experimental results in steady-state conditions. Thermal capacitors C_{th0}, which depend on the volume of the heat sink and the specific heat, have been calculated analytically.

3.2.1. Static thermal network parameters In order to specify the static parameters R_{c0}, R_{v0} and T_{ext}, the MicroPelt's heat sink has been connected only to the MiniPeltier. The
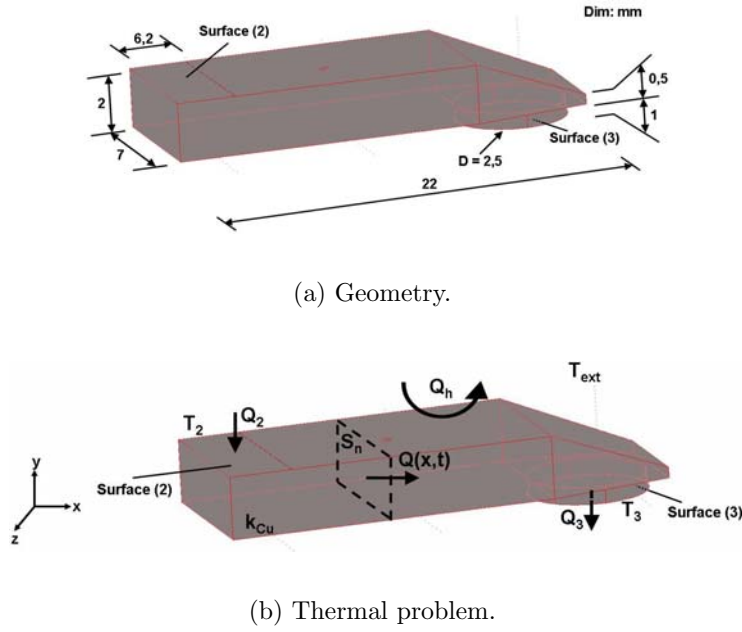
(a) Geometry.

(b) Thermal problem.

Figure 6. MicroPelt's heat sink.

Figure 7. Thermal network of the MicroPelt's heat sink [37].

identification method is based on the measurement of T_3 in function of the current in the MiniPeltier, i_{mP}.

As the MicroPelt is not fixed on its heat sink, surface (3) presents a convection heat transfer condition. Heat flux Q_3 is thus:

$$Q_3 = h_w S_3 (T_3 - T_w), \tag{1}$$

where $h_w = 1500$ W/m^{2}K is the convection coefficient in water and $S_3 = 4.9$ mm^2 is surface (3).

According to the figure 7, temperatures T_2 and T_3 in steady-state can be written as:

$$T_2 - T_{ext} = \frac{R_{v0}\left((R_{c0} + R_{v0})Q_2 - R_{v0}Q_3\right)}{R_{c0} + 2R_{v0}}, \tag{2}$$

$$T_3 - T_{ext} = \frac{R_{v0}\left(R_{v0}Q_2 - (R_{c0} + R_{v0})Q_3\right)}{R_{c0} + 2R_{v0}}. \tag{3}$$

Introducing (1) in (3), Q_2 can be expressed as a function of R_{c0}, R_{v0}, T_{ext}, T_3 and T_w:

$$\begin{aligned}
Q_2(T_3) &= \frac{R_{c0} + 2R_{v0}}{R_{v0}^2}(T_3 - T_{ext}) \\
&+ \frac{R_{c0} + R_{v0}}{R_{v0}}h_w S_3(T_3 - T_w)
\end{aligned} \tag{4}$$

Inserting (1) and (4) in (2), T_2 is defined as a function of R_{c0}, R_{v0}, T_{ext}, T_3 and T_w:

$$\begin{aligned}
T_2(T_3) &= \frac{R_{v0}}{R_{c0} + 2R_{v0}}((R_{c0} + R_{v0})Q_2(T_3) \\
&- R_{v0}h_w S_3(T_3 - T_w)) + T_{ext}
\end{aligned} \tag{5}$$

Considering the behavior of the thermal network in figure 5, Q_2 can be expressed as a function of $T_1 = T_a$ and T_2:

$$Q_2(T_3) = -(\alpha_{mP}i_{mP} + 1/R_{THmP})T_2(T_3) + R_{mP}i_{mP}^2/2 + T_a/R_{THmP} \tag{6}$$

T_3 is the solution of (6) defined as a function of i_{mP}, R_{c0}, R_{v0}, T_{ext}, T_1 and T_w. Parameters R_{c0}, R_{v0} and T_{ext} can be thus calculated from a non-linear system of equations with three different experimental couples (i_{mP}, T_3), knowing temperatures and T_w and T_a, and MiniPeltier's parameters α_{mP}, R_{mP} and R_{THmP} done in table 2.

To perform the experimental measurements, the submerged freeze microgripper has been tested in real use conditions: the forced convection system and the MiniPeltier stay completely in air, while the MicroPelt's heat sink is partially submerged. The MicroPelt has been removed allowing direct measurements on surface (3). For an applied current i_{mP}, we measure temperature T_3 until its steady-state using a microthermocouple. Temperatures $T_a = 295.5$ K and T_w were also measured with a thermometer and a microthermocouple, respectively. Experimental ordered triple (i_{mP}, T_3, T_w) measured are shown in table 3.

Parameters R_{c0}, R_{v0} and T_{ext} verifying theses conditions are presented in table 4.

3.2.2. Analytical identification of the thermal capacitor The thermal capacitor C_{th0} depends on the geometry of the heat sink and its physical properties:

$$C_{th0} = \frac{\rho C_p V}{2} \tag{7}$$

Table 3. Experimental static values.

i_{mP} (A)	T_3(K)	T_w (K)
0.1	281.2	274.5
0.4	274.2	274.5
0.7	272.2	273.8

where $\rho = 8960$ kg/m^3 is the density of the copper heat sink, $C_p = 385$ J/(kg.K) is the specific heat, and $V = 278$ mm^3 is the volume according to its geometry (see figure 6(a)).

The result obtained is shown in table 4.

Table 4. Parameters of the MicroPelt's heat sink thermal network.

Parameter	Value	Unit
Thermal conduction resistance R_{c0}	3.3	K/W
Thermal convection resistance R_{v0}	36.1	K/W
Thermal capacitor C_{th0}	0.48	J/K
External temperature T_{ext}	281.1	K

Thermal networks of the Peltier elements (MiniPeltier and MicroPelt) and the heat sink (figure 5 and figure 7) are completely defined. A model of the ice generation is proposed in the next section.

4. Thermal networks of ice generation

The thermal model of ice generation describes heat exchanges between MicroPelt's cold face and water. On the one hand, the evolution of heat flux Q_4 and temperature T_4 at the MicroPelt's cold face depend on the applied current $i_{\mu P}$ and the temperature T_3 at the MicroPelt's hot face; on the other hand, the evolution of the ice thickness H_{ice} depends on Q_4 and T_4. Here, two cases are studied: (i) thermal problem when an ice microvolume is grown, (ii) thermal problem at the MicroPelt's cold face without ice. Next analysis deals with the thermal network in each case, and the equations describing the corresponding phenomenon.

4.1. Thermal problem with ice

The generation of ice is done when the temperature T_4 at the cold face of the MicroPelt and the melting point of water T_f have the same value ($T_4 = T_f$). As the thickness of the ice is very small, this temperature is considered uniform at temperature T_f:

$$T_4 = T_5 = T_f \tag{8}$$

where temperature T_5 is the temperature of the ice in contact with water.

We consider that this surface is a circle instead a square to build an analytical model. Its diameter $d_{\mu P} = 812$ μm is calculated in order to have the same surface S_4 of the experimental system.

After experimental observations, we consider that the microvolume of ice has a spherical calotte geometry (figure 8). Its volume V_{ice} and the surface S_5 in contact with water are:

$$V_{ice} = \frac{\pi H_{ice}}{24}(3d_{\mu P}^2 + 4H_{ice}^2) \tag{9}$$

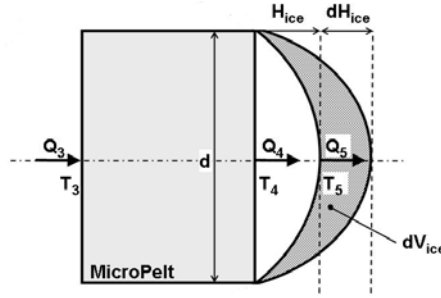$$S_5 = \frac{\pi}{4}(d_{\mu P}^2 + 4H_{ice}^2) \tag{10}$$

Figure 8. Geometry of the ice microvolume (lateral view).

The surface of the ice microvolume in contact with water has a heat convection flux Q_5 with the water:

$$Q_5 = \frac{1}{Z_{ice}}(T_f - T_w) \tag{11}$$

where $Z_{ice} = h_w S_5$ is a variable and non-linear thermal impedance which depends on height of the ice H_{ice} (see(10)).

The evolution of the ice's height is a function of the difference between Q_5 and Q_4, which is absorbed by latent heat:

$$\rho_{ice} L_f \frac{dV_{ice}}{dt} = Q_5 - Q_4 \tag{12}$$

where ρ_{ice} is the ice density and L_f is the water's latent enthalpy of fusion.

Considering (9) and (11), the temporal variation of ice thickness H_{ice} in relation with temperatures T_f and T_w, and heat flux Q_4 is:

$$\frac{dH_{ice}}{dt} = \frac{1}{\rho_{ice} L_f}\left(2h_w(T_f - T_w) - \frac{8Q_4}{\pi(d_{\mu P}^2 + 4H_{ice}^2)}\right) \tag{13}$$

This equation allows to calculate the height of the ice H_{ice} at every time t and thus to determine the variable impedance Z_{ice}.

4.2. Thermal problem without ice

As MicroPelt is completely submerged in water without ice ($H_{ice} = 0$), a convection heat transfer takes place between the MicroPelt's cold face and the medium:

$$Q_4 = \frac{1}{R_{v4}}(T_4 - T_w) \tag{14}$$

where $R_{v4} = 1/(h_w S_4)$ is the thermal convection resistance, h_w is the convective heat transfer coefficient of water, and $S_4 = \pi d_{\mu P}^2/4$ is the surface of the MicroPelt's cold face.

The thermal behavior at the MicroPelt's cold face without ice, can be thus represented as the equivalent electrical model in figure 9.

Modelling of thermal behavior at the MicroPelt's cold face and non-linear growing of the ice microvolume is summarized in figure 9. Parameters of these thermal networks are presented in table 5.
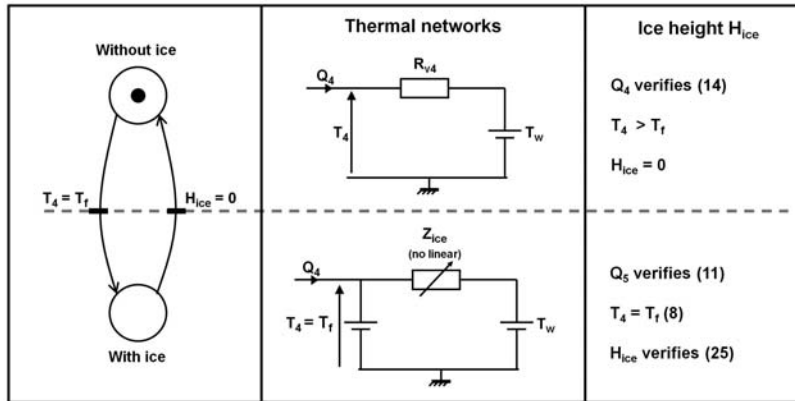

Figure 9. Thermal modelling of the ice generation using electrical analogy.

Table 5. Parameters of the ice thermal networks.

Parameter	Value	Unit
R_{v4}	1637	K/W
ρ_{ice}	920	kg/m^3
L_f	330	kJ/kg
T_f	273	K

5. Thermal network of whole system

One of the advantages of thermal modelling using electrical analogy is the possibility of connecting the thermal networks of different subsystems. Here, we use this advantage to construct the whole thermal network of the submerged freeze microgripper connecting
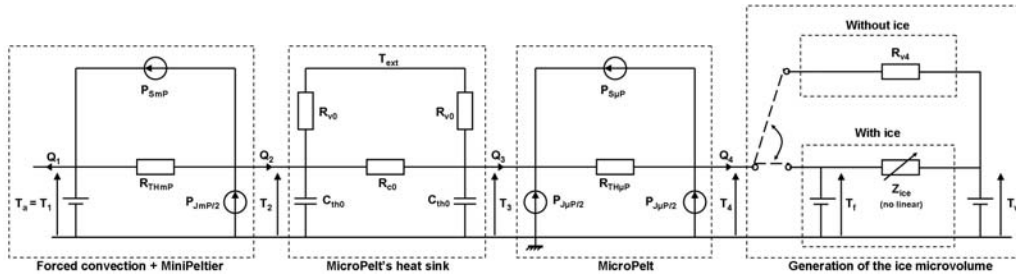
Figure 10. Thermal network of the submerged freeze microgripper.

the equivalent electrical models of its elementary components: the forced convection cooling system, the MiniPeltier, the MicroPelt's heat sink, the MicroPelt, and the ice microvolume. The thermal network of the submerged freeze gripper are depicted in figure 10. This thermal network let us modelling the ice generation as a function of the electrical currents $i_{\mu P}$ and i_{mP} of the MicroPelt and the MiniPeltier, respectively. It is able to provide easily a linear modelling of the ice microgripper which will be use to study the automatic control of this device. Next sections deals with the simulation of the whole thermal network and the experimental validation.

5.1. Simulation model

The thermal network of the submerged freeze microgripper has been simulated with Simulink$^{\text{TM}}$ and Matlab$^{\text{TM}}$, considering an ambient temperature $T_a = 295.5$ K, and a water temperature $T_w = 274.2$ K.

Figure 11 describes an example of a simulation result of the network presented in figure 10:

(a) temperatures T_3 and T_4 of the MicroPelt's hot face and cold face are stationary; MiniPeltier's current i_{mP} and MicroPelt's current $i_{\mu P}$ are zero ($i_{mP} = i_{\mu P} = 0$ A); and ice thickness is zero ($H_{ice} = 0$ μm);

(b) only the MiniPeltier is activated at 0.4 A ($i_{mP} = 0.4$ A). This value is always maintained in the following steps. Temperatures T_3 and T_4 reduces, T_4 stay always greater than melting point T_f: ice thickness stays zero ($H_{ice} = 0$ μm);

(c) the MicroPelt is activated at 0.5 A ($i_{mP} = 0.4$ A, $i_{\mu P} = 0.5$ A). Temperature T_4 falls and reaches melting point T_f ($T_4 = T_f = 273$ K) producing ice generation ($H_{ice} > 0$ μm). Temperature T_3 increases slightly because of the MicroPelt;

(d) the MicroPelt is switched off ($i_{\mu P} = 0$ A), ice thaws and H_{ice} reduces. Temperatures T_4 stays at melting point T_f while $H_{ice} > 0$ μm. Temperature T_3 reduces slightly because of the MiniPeltier;

(e) the ice microvolume is completely thawed ($H_{ice} = 0$ μm) and T_4 grows. Electrical currents i_{mP} and $i_{\mu P}$ are maintained to their previous values ($i_{mP} = 0.4$ A, $i_{\mu P} = 0$ A).
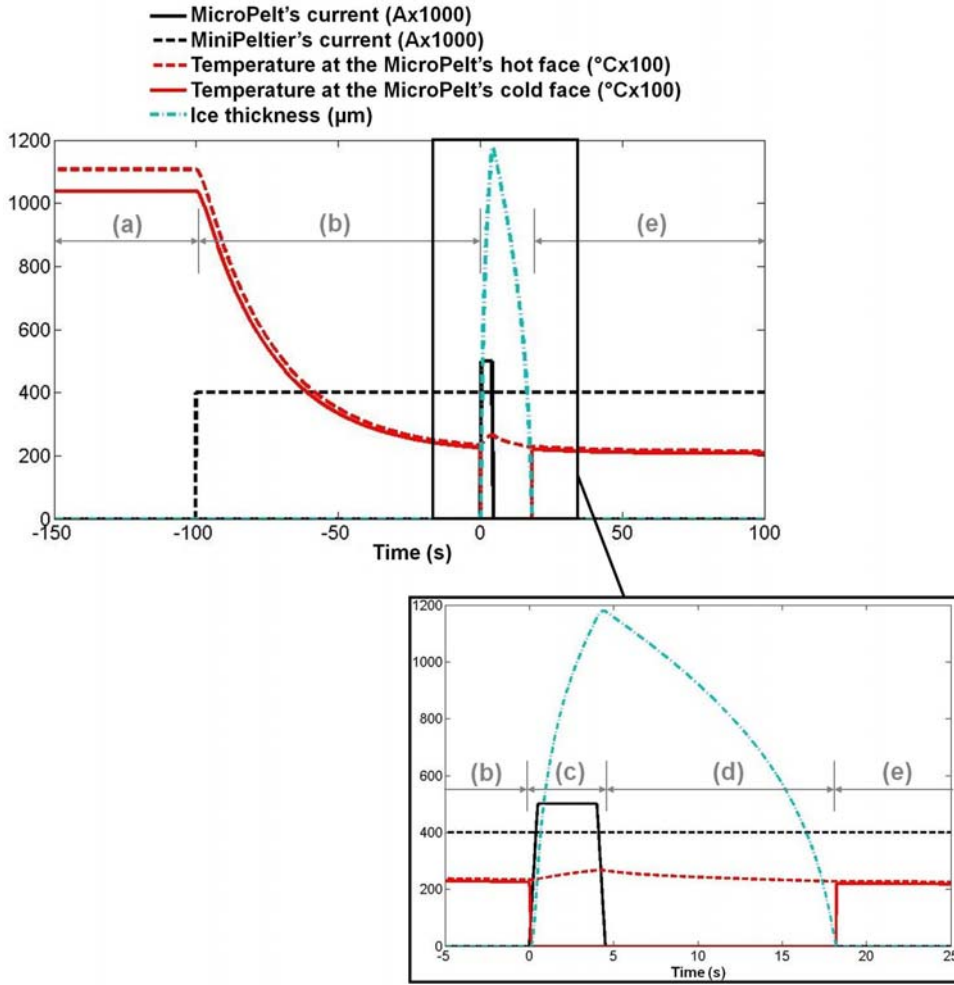
Figure 11. Evolution of MicroPelt's current $i_{\mu P}$, MiniPeltier'current i_{mP}, temperatures T_3 and T_4 at the MicroPelt's hot face and cold face, respectively, and ice thickness H_{ice}. Signals obtained simulating the thermal network of the submerged freeze gripper.

5.2. Experimental behaviour

The experimental behavior of the submerged freeze gripper (upper view) has been filmed with CDD camera. Ice thickness H_{ice} is manually measured for every image taken. Figure 12 depicted the experimental dynamic evolution of the electrical currents i_{mP} and $i_{\mu P}$, and temperature T_4 form MicroPelt activation:

(a) MiniPeltier's and MicroPelt's currents are zero $i_{mP} = i_{\mu P} = 0$ A, and temperatures are stationary;

(b) the MiniPeltier is activated ($i_{mP} = 0.9$ A; $i_{\mu P} = 0.5$ A) to reduce MicroPelt's heat sink temperature. This current is strongly dependent on experimental conditions (submerged surfaces, temperature and volume of water, etc.). During this experimentation, required i_{mP} is bigger than this one required during simulation.

This value is maintained during all the experimentation. MicroPelt's current stays at zero ($i_{\mu P} = 0$ A);

(c) MicroPelt is activated ($i_{\mu P} = 0, 5$ A), water is locally get cold, but a supercooling phenomenon appears. Simulation does not consider this phenomenon, which induces a crystallization delays. During simulations, ice generation begins immediately after MicroPelt's activation and T_f is at 273 K;

(c') ice generation takes place. First crystallization appears at time t_4, some seconds after current $i_{\mu P}$ sets up to 0.5 A, at t_3. This phenomenon, caused by supercooling as explained, is not observed during following crystallizations;

(d) MicroPelt's current is inversed ($i_{mP} = -0.5$ A), MicroPelt's hot face warms up and ice microvolume thaws;

(e) in order to repeat ice generation and thawing, a square signal ± 0.5 A is applied to $i_{\mu P}$.
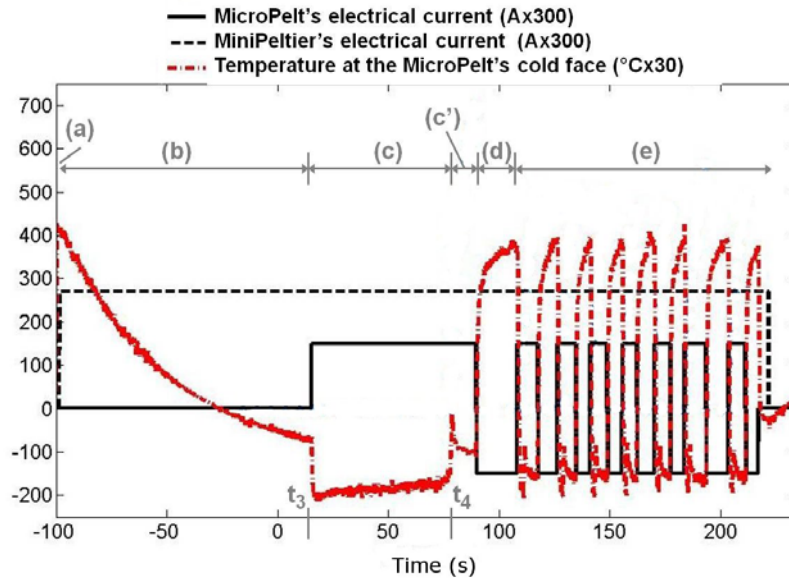

Figure 12. Experimental sequence of ice generation: evolution of ice thickness H_{ice}, MiniPeltier's or MicroPelt's currents i_{mP} and $i_{\mu P}$, and temperature at the MicroPelt's cold face T_4.

For the micromanipulation operations described in [10], the cycle time for pick up and release the micro-object is 10 s. This time could be reduced controlling the thickness of the ice droplet via, for instance, a visual control system directly acting over Peltier module's currents. Moreover, the reduction of the size of both gripper and micro-object could enable the reduction of the thermal inertia, and thus the improvement of the time response.

5.3. Comparison between experimental and simulated ice

In order to validate the thermal network of the submerged freeze microgripper, measured and simulated ice thickness H_{ice} have been compared. For this validation, temperature at the MicroPelt's hot face T_3 has been fixed at 295 K at the simulator. Figure 13 shows the results of the comparison. Experimental and simulated behaviors follow the same trends. Three major differences can be identified.
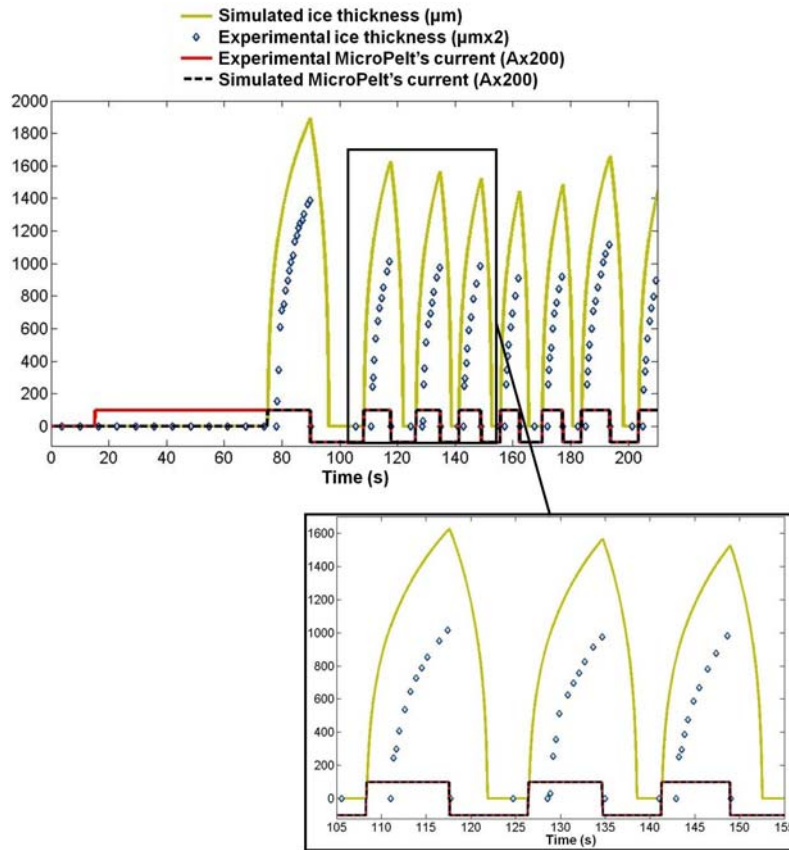

Figure 13. Comparison between ice thickness H_{ice} and electrical current $i_{\mu P}$ obtained experimentally and simulating the thermal network of the submerged freeze microgripper.

First, simulation of the submerged freeze microgripper's thermal network imposes the ice generation immediately after MicroPelt's activation. For this reason, during the first crystallization, simulated current $i_{\mu P}$ is voluntary delayed against experimental $i_{\mu P}$ searching that measured and experimental H_{ice} begin at the same time. This first crystallization is not representative of the sequential use of the gripper. During the following crystallizations, both, simulated and experimental currents have the same dynamics.

Second, thawing model does not represent the real phenomenon. During experiments, ice is detached of the MicroPelt's cold face, contrary to simulation, where H_{ice} decreases continuously.

Third, it is obvious that simulated H_{ice} is bigger than experimental H_{ice}. In fact, thermal networks of Peltier modules does not consider electrical contact resistances. These losses become bigger than Peltier effect showing that experimental heat flux provided by Peltier modules is lower than simulated heat flux: simulated ice microvolume is generated faster than experimental ice microvolume.

Fourth, the geometry of ice droplet has been modelled as a spherical calotte overcoming only MicroPelt's cold face. Experimentally, ice volume is bigger than modelled volume. Consequently, real ice droplet takes more time to grow than simulated ice droplet.

Summarizing, the network model does not consider supercooling phenomenon, real thawing process, and contact resistances. Furthermore, simulated geometry of the ice droplet is smaller than real geometry. The two last limitations produce that simulated ice grows faster than experimental ice. In order to improve the network model, measurement concerning junction resistances and the real ice microvolume must be done.

Despite these differences, thermal network of the simulated submerged freeze microgripper lets follow ice generation in real time as a function of electrical currents of Peltier modules.

6. Conclusion

Modelling of complex thermal problems using electrical analogy presents severals advantages as flexibility, precision real time calculation and easy connection of various models. We have thus developed a dynamical thermal network of the submerged freeze microgripper proposed in this article. This thermal network is based on the thermal networks of every elementary component: forced convection system, MiniPeltier, MicroPelt's heat sink, and the MicroPelt. Identification of the thermal network's parameters has been done by analytical calculations or based on experimentations. Thermal network of the submerged freeze microgripper is completed with an original non-linear thermal network of the ice generation. Connecting all these networks, we have built the thermal network of the whole submerged freeze microgripper. This network lets to observe real time ice generation as a function of electrical currents of both Peltier's modules. Further work will deal with the use of this thermal network to design control strategies in order to enable automatic microgripping.

Acknowledgments

References

[1] BS. Kim, J-S. Park, Moon C., G-M. Jeong, and Ahn H-S. A precision robot with modular actuators and mems micro gripper for micro system assembly. *Journal of Mechanical Science and Technology*, 22:70–76, 2008.

[2] T. Watanabe, N. Fujino, and Z. Jiang. Micromanipulation using squeeze effect. In *Proc. of IEEE IROS*, volume 4, pages 3357–3362, Japan, 2004.

[3] V. Sariola, Q. Zhou, and H. N. Koivo. Hybrid microhandling: a unified view of robotic handling and self -assembly. *Journal of Micro-Nano Mechatronics*, 4:5–16, 2008.

[4] M. Savia, Q. Zhou, and H. N. Koivo. Simulating adhesion forces between arbitrarily shaped objects in micro/nano-handling operations. In *Proc. of IEEE/RSJ IROS*, pages 1772–1727, Japan, 2004.

[5] Q. Zhou, B. Chang, and H. N. Koivo. Ambient environment effects in micro/nano handling. In *Proc. of IEEE IWMF*, pages 146–151, Shangai, China, October 2004.

[6] A. M. Petrina. Micromanipulation in robotics. *Automatic Documentation and Mathematical Linguistics*, 42(1):66–70, 2008.

[7] M. Gauthier, S. Régnier, P. Rougeot, and N. Chaillet. Analysis of forces for micromanipulations in dry and liquid media. *Journal of Micromechatronics*, 3(3-4):389–413, 2006.

[8] J. Dejeu, P. Rougeot, M. Gauthier, and W. Boireau. Reduction of micro-object's adhesion using chemical functionnalisation. *MicroNano Letters*, 4(2):74–79, 2009.

[9] J. Dejeu, M. Gauthier, P. Rougeot, and W. Boireau. Adhesion forces controlled by chemical self-assembly and ph, application to robotic microhandling. *ACS Applied Materials & Interfaces*, 1(9):19661973, 2009.

[10] B. López-Walle, M. Gauthier, and N. Chaillet. Principle of a submerged freeze gripper for microassembly. *IEEE Transactions on Robotics*, 24(4):897–902, 2008.

[11] A. Kochan. European project develops "ice" gripper for micro-sized components. *Assembly Automation*, 17(2):114–115, 1997.

[12] G. Seliger, J. Stephan, and S. Lange. Hydroadhesive gripping by using peltier effect. In *Proc. of IMECE*, pages 3–8, USA, November 2000.

[13] J. Liu, Y-X. Zhou, and T-H. Yu. Freeze tweezer to manipulate mini/micro objects. *Journal of Micromechanics and Microengineering*, 14(2):269–276, February 2004.

[14] C. Ru, X. Wan, X. Ye, and S. Guo. A new ice gripper based on thermoelectric effect for manipulating micro objects. In *Proc. of IEEE International Conference of Nanotechnology*, pages 438–441, August, 2007. Hong Kong.

[15] M. Lang, D. Tichem and F. Warner. An industrial prototype of a liquid solidification based micro-gripping system. In *Proc. of IEEE International Symposium on Assembly and Manufacturing*, pages 227–232. USA, July 2007.

[16] Y. Yang, J. Liu, and Y-X. Zhou. Convective cooling enabled freeze tweezer for manipulating micro-scale objects. *Journal of Micromechanics and Microengineering*, 18(9):095008–095017, 2008.

[17] M. Tichem, D. Lang, and B. Karpuschewski. A classification scheme for quantitative analysis of micro-grip principles. *Assembly Automation*, 24(1):88–93, 2004.

[18] F. Biganzoli, I. Fassi, and C. Pagano. Development of a gripping system based on a capillary force. In *Proc. of IEEE ISATP*, pages 36–40, Canada, 2005.

[19] P. Lambert and A. Delchambre. A study of capillary forces as a gripping principle. *Assembly automation*, 25(4):275–283, 2005.

[20] D. Schmid, S. Koelemeijer, J. Jacot, and P. Lambert. Microchip assembly with capillary gripper. In *Proc. of IEEE IWMF*, France, 2006.

[21] A. Vasudev and J. Zhe. A capillary microgripper based on electrowetting. *Applied Physics Letters*, 93:103503 (3pp), 2008.

[22] B. Bhushan and X. Ling. Manipulating microobject by using liquid droplet as a transporting

vehicle. *Journal of Colloid and Interface Science*, 329:196–201, 2009.

[23] S. K. Chung and S. K. Cho. 3-d manipulation of millimeter- and micro-sized objects using an acoustically excited oscillating bubble. *Microfluidics and Nanofluidics*, 6:261–265, 2009.

[24] K. J. Obata, T. Motokado, S. Saito, and K. Takahashi. A scheme for micro-manipulation based on capillary force. *Journal of Fluid Mechanics*, 498:113–121, 2004.

[25] S. Saito, T. Motokado, K. J. Obata, and K. Takahashi. Capillary force with a concave probe-tip for micromanipulation. *Applied Physics Letters*, 87:234103 (3pp), 2005.

[26] B. Bhushan and X. Ling. Integrating electrowetting into micromanipulation of liquid droplets. *Journal of Physics: Condensed Matter*, 20:485009 (10pp), 2008.

[27] J. Stephan and G. Seliger. Handling with ice - the cryo-gripper, a new approach. *Assembly Automation*, 19(4):332–337, 1999.

[28] D. Lang, M. Tichem, and S. Blom. The investigation of intermediates for phase changing micro-gripping. In *Proc. of IEEE IWMF*, France, October 2006.

[29] J. P. Holman. *Heat transfer*. Mac Graw Hill, 1990.

[30] J. G. Vián, D. Astrain, and M. Domínguez. Numerical modelling and a design of a thermoelectric dehumidifier. *Applied Thermal Engineering*, 22:407–422, 2002.

[31] A. Alhama, F. Campo. Network simulation of the rapid temperature changes in the composite nozzle wall of an experimental rocket engine diuring a ground firing test. *Applied Thermal Engineering*, 23:37–47, 2003.

[32] C. Cristofari, G. Notton, and A. Louche. Study of the thermal behaviour of a production unit of concrete structural components. *Applied Thermal Engineering*, 24:1087–1101, 2004.

[33] B. Borovic et al. Method for determining a dynamical state-space model for control of thermal mems devices. *Journal of Microelectromechanical Systems*, 14(5):961–970, 2005.

[34] J. Zueco and A. Campo. Network model for the numerica simulation of transient radiative transfer process between the thick walls of enclosures. *Applied Thermal Engineering*, 26:673–679, 2006.

[35] M. J. F. Zeman, E. V. Bordatchev, and G. K. Knopf. Design, kinematic modeling and performance testing of an electro-thermally driven microgripper for micromanipulation applications. *Journal of Micromechanics and Microengineering*, 16:1540–1549, 2006.

[36] D. Lang, I. Kurniawan, M. Tichem, and B. Karpuschewski. First investigations on force mechanisms in liquid solidification micro-gripping. In *Proc. of ISATP*, pages 92–97, July 19-21 2005.

[37] B. López-Walle, M. Gauthier, and N. Chaillet. Dynamic modelling of a submerged freeze microgripper using a thermal network. In *IEEE/ASME AIM*, Switzerland, 2007.